LIMNOLOGY and OCEANOGRAPHY

ASLO

Limnol. Oceanogr. 66, 2021, 2779–2796

doi: 10.1002/lno.11788

Pico- and nanoplankton communities on a near to offshore transect along the continental shelf of the northwestern Gulf of Mexico in the aftermath of Hurricane Harvey

Gulce Kurtay,* **Hans J. Prevost**, **Beth A. Stauffer**
Department of Biology, University of Louisiana at Lafayette, Lafayette, Louisiana

Abstract

Hurricane Harvey delivered over 124 trillion liters of freshwater to the Texas–Louisiana coast and the northwestern Gulf of Mexico (GOM) in late August-early September 2017. Environmental conditions, size-fractionated phytoplankton biomass, and pico- and nanoplankton abundances (picocyanobacteria, picoeukaryotes, autotrophic, and heterotrophic nanoplankton) were characterized along nearshore-offshore transects prior to Hurricane Harvey (late July 2017) and in the 3 weeks to 6 months following the storm (September 2017 to March 2018). To understand the extent to which observed changes in the aquatic environment and plankton communities could be attributed to Hurricane Harvey (vs. seasonal or interannual variability), salinity, temperature, and phytoplankton biomass from historical data (2006–2018) were also analyzed. Nearshore stations from September and October 2017 showed significantly lower salinities and overall phytoplankton biomass compared to historical data. Inorganic nitrogen concentrations were minimal in October. Pico- and nanoplankton abundances were lower in September and October than prior to the storm, with the exception of picocyanobacteria. In contrast, post-storm biomass at mid-shelf stations was within the historical average, while pico- and nanoplankton abundances were higher. Offshore stations showed little change in biomass or abundances following the storm. Pre-storm assemblages of pico- and nanoplankton in July 2017 were distinct from those in post-storm months, and variance in these assemblages and specific group abundances was tied to inorganic nutrients, salinity, and temperature. These results point to significant changes in important members of the plankton that occurred in GOM continental shelf waters following a major hurricane, with important implications for oceanic food webs and biogeochemical cycles.

Tropical cyclones, such as hurricanes, tropical depressions and storms, and typhoons have significant ecological effects on coastal systems, changing the population density and evenness of organisms ranging from vegetation to fauna with wind velocity, storm duration, and rainfall (Ackerman et al. 1991). Aquatic ecosystems are subject to direct impacts of tropical cyclones from wind, rainfall, and changes in water circulation, which trigger physical effects including water mixing, changes in stratification, and upwelling (Jullien et al. 2012). Most of this study has focused on impacts in estuaries (e.g., Valiela et al. 1998; Peierls et al. 2003; Hu and Muller-Karger 2007; and others), where tropical cyclones winds and river input can induce vertical mixing and result in the increase of suspended materials in shallow water columns (Hu & Muller-Karger 2007). The increased rainfall also accelerates river input which leads to hyposaline, high nitrogen and phosphorus conditions in the system (Peierls et al. 2003). Research on storm effects further offshore have largely focused on direct impacts of wind, circulation, sea surface temperature (SST) and features that can be identified with remote sensing or buoy-based systems (e.g., Babin et al. 2004; Sanford et al. 2007; Zheng and Tang 2007; and others). In these offshore waters, strong, rotational winds from tropical cyclones can drive upwelling, thus introducing higher salinity, cooler, nutrient-rich bottom waters to the surface (Zheng and Tang 2007). Deepening of the mixed layer due to curl-induced upwelling also is a common response to direct wind effects in pelagic systems (Babin et al. 2004). In the aftermath of many

*Correspondence: gulce.kurtay1@louisiana.edu

Additional Supporting Information may be found in the online version of this article.

Author Contribution Statement: GK carried out sample processing, data analyses, and interpretation, and led manuscript preparation. HJP contributed to sample processing and analyses and provided comments to the manuscript. BAS conceived of the study with project collaborators, carried out its design and sampling, and participated in manuscript preparation and revision. All authors read and approved the final manuscript.

storms, such physical and biogeochemical changes can stimulate growth in phytoplankton biomass (Zheng and Tang 2007) and/or phytoplankton blooms (Han et al. 2012). However, the extent to which these effects progress over longer-term (weeks to months) and larger spatial scales (100 s of kilometers) that are relevant for secondary and fisheries productivity remain important ecological questions.

Tropical cyclone effects on ecosystems can vary with each storm, and factors like pre-storm conditions and storm characteristics play a significant role in this variability (Hogan et al. 2020). Wetz and Paerl (2008a), for example, found that hurricanes were more likely to lead to increased phytoplankton biomass in the Neuse River Estuary when the water column was stratified, and surface nutrients were limiting prior to the storm. In contrast, water columns that were well-mixed and with high surface nutrient concentrations prior to a storm typically did not experience increases in phytoplankton biomass following hurricanes (Wetz & Paerl, 2008a). As tropical cyclones are predicted to continue to intensify with climate change (Collins et al. 2019), there is a pressing need to better understand the ecological effects of these extreme weather events across a range of antecedent conditions and storm characteristics on aquatic ecosystems.

While understanding the effects of tropical cyclones on phytoplankton is an ongoing area of research, much of that work has quantified only biomass (e.g., Zheng and Tang 2007; Han et al. 2012; Lü et al. 2020, and others). Fewer studies have resolved effects on composition of phytoplankton communities, with important exceptions (e.g., Chang et al. 1996; Peierls et al. 2003; Anglès et al. 2015; Paerl et al. 2020; Wachnicka et al. 2020). Results of studies that have resolved effects on communities have yielded important insights. For example, Anglès et al. (2015) documented the effects of four tropical cyclones on coastal phytoplankton communities in the Guadalupe, Mission-Aransas, and Nueces estuaries in the GOM. Storm impacts were categorized as either (1) storm surge and winds or (2) heavy rain, freshwater discharge, and decreased salinity. Increases in diatom abundances were linked to storm surge, while increases in dinoflagellate and other flagellates were associated with freshwater discharge (Anglès et al. 2015). However, the responses of the smaller pico- and nano-sized groups to tropical cyclone events are even less well-resolved. One multistorm study conducted off the coast of Taiwan considered the effects on the picocyanobacteria taxa, *Synechococcus*, abundances of which sequentially decreased and then recovered within days, while biomass of larger groups (> 5 μm) continued to increase following multiple tropical cyclones (Chang et al. 1996). Recently, Paerl et al. (2020) investigated the effects of storms on picophytoplankton biomass and communities by looking at the long-term effects of Hurricane Florence and other precipitation events over a 1.5-year period in the Neuse River Estuary. This study revealed a reduction in picophytoplankton biomass following 2 weeks of storms and subsequent picoeukaryote blooms that occurred sometimes several months following precipitation events (Paerl et al. 2020).

The effects of tropical cyclones on pico- and nanoplankton biomass or communities in shelf and oceanic waters of GOM has not been studied in depth or for periods following storm events, despite these groups dominating primary production in this system (Liu et al. 2004; Chakraborty and Lohrenz 2015). In oligotrophic GOM waters, 46% of carbon biomass is attributable to autotrophs (primarily picocyanobacteria, picoeukaryotes) and 54% to heterotrophic bacteria in winter months (Linacre et al. 2015). Along the Texas–Louisiana shelf, cyanobacteria and larger diatoms (nano- and micro-size classes) dominate, whereas picocyanobacteria and other smaller-sized pelagophytes and prymnesiophytes (also pico- and nanoplankton) dominate surface waters off the continental slope (Lambert et al. 1999). Success of these groups is strongly influenced by specific combinations of temperature, salinity, and nutrients in both coastal and offshore GOM waters (Williams et al. 2015; Williams and Quigg 2019).

Understanding the effects of tropical cyclones on plankton communities, especially pico- and nanoplankton populations, is key, given their important ecological roles in oceanic food webs and biogeochemical cycling. Overall productivity and diversity of higher trophic levels and trophic energy efficiency are dependent on quantity and quality of resources at the base of the food web (Dickman et al. 2008). Extreme event impacts on primary producers can lead to changes in food web structure and trophic cascades that impact higher trophic levels (e.g., in planktivorous flying fish, Fiedler et al. 2013). For this reason, it is essential to understand how tropical cyclones induce change in pico- and nanoplankton biomass and community structure.

This article investigates how standing stocks and assemblage composition of pico- and nanoplankton changed following Hurricane Harvey, a Category 4 hurricane that made landfall along the Texas–Louisiana coast on August 24–28, 2017. Hurricane Harvey was notable among hurricanes in the region for its record-breaking rainfall of over 1.5 m in Grove and Nederland, TX (Blake and Zelinsky 2018). This precipitation resulted in freshwater input exceeding three times the volume of Galveston Bay (11.1×10^9 m^3), which decreased the salinity in the bay to near zero for 4 days following the storm (Du et al. 2019a). Along with this freshwater, significant amounts of organic carbon and sediment were delivered, adding the equivalent of 18 years of average sediment load to Galveston Bay (Du et al. 2019a). Significant amounts of total organic carbon (tDOC, 5.2×10^6 kg) and suspended particulate matter ($\sim 314.7 \times 10^6$ kg) were rapidly exported from the Galveston estuary and introduced to the continental shelf of the northwestern GOM (D'Sa et al. 2018). Within Galveston Bay, increases in diatom, chlorophyte, and dinoflagellate abundances were observed in the 4 weeks following the storm as well as increases in heterotrophic bacteria of terrestrial

origin (Steichen et al. 2020). Through a series of cruises conducted prior to and in the weeks and months following Hurricane Harvey, the current study resolves how phytoplankton standing stocks and, specifically, pico- and nanoplankton populations were affected by this extreme storm event in nearshore waters (< 50 km from shore), on the Texas–Louisiana shelf (50–130 km from shore) and further offshore (> 150 km from shore). This study fills a critical knowledge gap in our understanding of the effects of tropical cyclones on the smallest members of plankton communities that form the base of oceanic food webs and on spatial and temporal scales that affect food web interactions and secondary and fisheries production in the GOM.

Methods

Study area

The study area is located on the Texas–Louisiana continental shelf in the northwestern GOM, extending from near the mouth of Galveston Bay to > 200 km offshore (Fig. 1; Table 1). Stations sampled ranged from the nearshore (water depth 16 m) to offshore (water depth > 1000 m, Table 1). Stations were sampled on cruises in July, September, October 2017 and January and March 2018 (Table 2). The July 2017 samples (Stations 2, 6, and 10a) were collected as part of the Gulf of Mexico Ecosystems and Carbon Cruise (GOMECC-3) aboard the NOAA Ship Ronald H. Brown (https://www.aoml.noaa.gov/ocd/gcc/GOMECC3/). Station 10a, sampled on the July cruise, was 35 km away from Station 10, which was sampled October 2017–March 2018. September 2017 samples were collected as part of the Southeast Area Monitoring and Assessment Program (SEAMAP) cruise aboard the NOAA Ship Gordon Gunter (https://www.gsmfc.org/seamap.php). In October 2017, January 2018, and March 2018 samples were collected on cruises aboard the R/V Point Sur (October 2017) and R/V Pelican (January and March 2018).

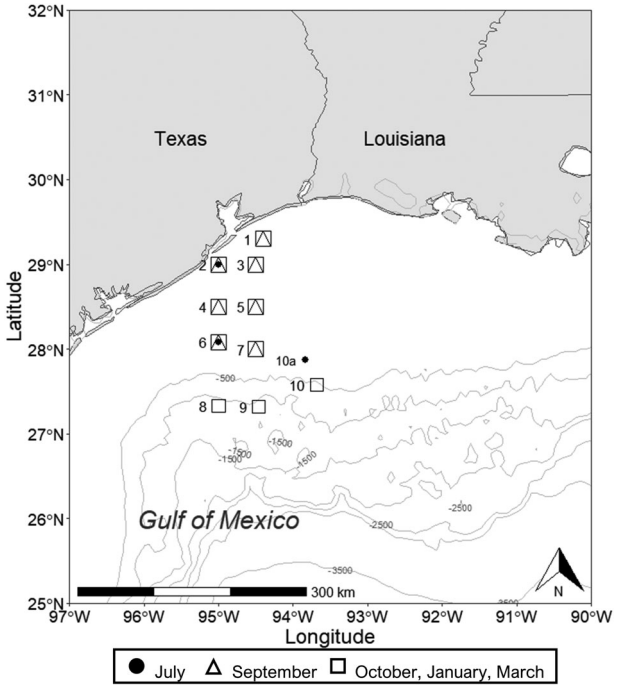

Fig. 1. Stations sampled in the northwestern Gulf of Mexico as part of the study. Different symbols represent months of sampling: July 2017 (circle); September 2017 (triangle); October 2017, January, and March 2018 (square). TABS Buoy B (not shown for clarity of map) is located 8 km southeast of Station 2. Station 10a, sampled in July 2017, is located 35 km from Station 10 (sampled in October, January, and March).

Sample collection and processing

Cruise-based samples were collected 4 weeks before (late July-early August 2017) and 3 weeks (September 2017), 2 months (October 2017), 4 months (January 2018), and 6 months (March 2018) following Hurricane Harvey. Environmental data were collected from the water column with a CTD instrument (Seabird Scientific SBE 911 Plus) equipped with sensors measuring: salinity, density (kg m^{-3}), temperature (°C), chlorophyll-*a* (Chl-*a*) fluorescence, colored dissolved organic matter (CDOM) fluorescence, and photosynthetically active radiation (PAR; μmol photons $m^{-2}s^{-1}$). All CTD casts were conducted between sunrise and sunset. Chl-*a* fluorescence values from Stations 2 and 4 in October were anomalously high and were back-corrected based on the linear relationship ($R^2 = 0.64$; $y = 1.45x + 0.04$) between Chl-*a* fluorescence and extracted Chl-*a* concentrations (*see* below for more details on extracted Chl-*a* samples). PAR data at Station 2 and CDOM fluorescence data at Stations [6, 7, and 8] in October were not used due to uncertainty in data quality. Water column stratification was quantified using the Brunt-*Väisälä* frequency (N^2; IOC et al. 2010). Absolute salinity (SA) and conservative temperature (CT) values were calculated from potential salinity and potential temperature measured by the CTD. Pressure (p) and latitude were measured from the CTD, and gravitational acceleration (g) was calculated from latitude. All necessary conversions and calculations for N^2 were computed using the "gsw" (version 1.0-5; Kelley and Richards 2017) package in R software. The attenuation coefficient (K_{dPAR}) was calculated from the PAR measurements from CTD casts in October to March by using the Boegert–Lambert Law equation (McPherson and Miller 1987). For the offshore, deep stations, K_{dPAR} was calculated using data from ≤ 150 m depth for consistency with the shallower stations.

Discrete water samples were obtained from Niskin bottles at varying depths guided by fluorescence readings to target the subsurface chlorophyll maximum ("Chl-max," if present), below the Chl-max and/or at the bottom of the water column ("Deep"), and in the upper 5 m ("Surface"). Samples for inorganic nutrient analyses ($NO_2 + NO_3$, PO_4, SiO_2) were collected from Niskin bottles at 2–3 depths per station on cruises in July 2017, October 2017, January 2018, and March 2018. Samples for NH_4 analyses were also taken on the October 2017–March 2018 cruises. No nutrient data are available for September

Table 1. Station information indicating latitude, longitude, distance from shore (km), and maximum water column depth (m) as measured from CTD altimeter.

Station #	Latitude	Longitude	Distance from shore (km)	Maximum water depth (m)	Month sampled (2017–2018)
1	29.30	−94.39	26	16	Sept, Oct, Jan, Mar
2	29.00	−95.00	14	18	Jul, Sept, Oct Jan, Mar
3	29.00	−94.50	44	20	Sept, Oct, Jan, Mar
4	28.50	−95.00	56	35	Sept, Oct, Jan, Mar
5	28.50	−94.50	88	38	Sept, Oct, Jan, Mar
6	28.08	−95.00	96	63	Jul, Sept, Oct, Jan, Mar
7	28.00	−94.50	130	72	Sept, Oct, Jan, Mar
8	27.33	−95.01	167	1000	Oct, Jan, Mar
9	27.32	−94.46	194	1107	Oct, Jan, Mar
10	27.58	−93.69	218	305	Oct, Jan, Mar
10a*	27.87	−93.83	183	95	Jul

*Station 10a was only sampled in July 2017 and is located 35 km from Station 10.

Table 2. Cruise information noting cruise dates, stations sampled, and samples collected for size-fractionated biomass (Chl-*a*), abundances via flow cytometry (flow) and inorganic nutrients (nutrients) on each cruise. Hurricane Harvey made landfall between 25 and 31 August 2017.

			Samples collected		
Cruise	Dates in study region	Stations sampled	Chl-*a*	Flow	Nutrients
July 2017	29–31 July 2017	2, 6, 10a	x	x	x
September 2017	22–24 September 2017	1–7	x*	x	
October 2017	30 October-3 November 2017	1–10	x	x	x
January 2018	8–12 January 2018	1–10	x	x	x
March 2018	19–23 March 2018	1–10	x	x	x

*Only whole seawater (WSW) Chl-*a* samples were collected in September 2017.

2017 due to sampling constraints. Nutrient samples from July 2017 were analyzed within 1 h through gas segmented continuous flow calorimetric analyses (Barbero et al. 2019). Nutrient samples from October 2017 to March 2018 were frozen at − 20 °C until analysis using an auto-analyzer method in the Wetland Biogeochemistry Analytical Services (WBAS) at Louisiana State University. EPA methods were used for nitrate and silicate analyses (Zhang and Berberian 1997; Zhang et al. 1997) and NH_4 samples from October–March were analyzed using the method of O'Dell (1996). Phosphate analytical methods differed slightly for samples analyzed from July 2017 (Zhang et al. 2000) vs. those collected in October 2017–March 2018 (Zimmerman and Keefe 1997). These two methods differ, primarily, in efficacy in high carbonate regions. Our study sites on the continental shelf are not characterized by high carbonate concentrations; as such, we do not expect the methodological differences to interfere with comparability of the phosphate data. Dissolved inorganic nitrogen (DIN) was calculated by the sum of nitrate (inclusive of nitrite) and ammonia concentrations. Dissolved inorganic nitrogen to inorganic silicate (DIN:Si), and dissolved inorganic nitrogen to inorganic phosphate (DIN:DIP) ratios were natural log (x + 1) transformed to represent ratios accurately (Isles, 2020).

Phytoplankton biomass was analyzed by fluorometry and cell abundances by flow cytometry. A functional group approach was used to characterize changes in biomass and community composition based on size (pico-, nano-, and microplankton) and trophic role (auto- vs. heterotroph; Wang et al. 2010; Christaki et al. 2011; Owen 2014; Ni et al. 2015). Phytoplankton biomass (as Chl-*a*) was fractionated according to size as whole seawater (WSW) and as < 20 μm, by pre-screening with 20 μm Nitex nylon mesh and subsequent gentle vacuum filtration in duplicate onto glass fiber filters (GFF). Filters were stored at − 20°C until analysis. Chl-*a* ($\mu g\, l^{-1}$) concentrations were measured by fluorescence (Turner Design 10-AU) using acidification with 10% hydrochloric acid (Parsons et al. 1984). Chl-*a* in the > 20 μm size fraction (representative of microphytoplankton) was calculated by subtracting the < 20 μm concentrations from the WSW concentrations.

Duplicate samples for nano- and picoplankton abundance were collected from Niskin bottles at each depth,

preserved in formalin at 1% final concentration in cryovials and stored at − 20 °C until analysis by flow cytometry (Becton-Dickinson FACSCalibur). Picoeukaryotes (PE) and picocyanobacteria (PC) were determined according to their autofluorescence in two channels (FL3, FL2) correlated with Chl-*a* and phycobiliprotein fluorescence, respectively, and size (Campbell 2001). Autotrophic (ANAN) and heterotrophic nanoplankton (HNAN) were determined based on unstained and then subsequently stained samples using existing methods (2×10^{-4} final concentration SYBR Green 1 for 30 min; Marie et al. 1997; Campbell 2001; Christaki et al. 2011). Each sample was run in duplicate for 2 min. Size-based groups were further determined using forward scatter (FSC) calibrated to polystyrene beads and checked against cultures of known size. Abundances (cells ml^{-1}) were calculated using known concentrations of reference counting beads (Becton Dickinson) which were run every 10 samples.

Historical data

Long-term salinity and temperature data (2013–2018) were accessed from the Texas Automated Buoy System (TABS), based out of the Geochemical and Environmental Research group at Texas A&M University (http://tabs.gerg.tamu.edu/). TABS Buoy B (29.22, −94.88) is located approx. 8 km from Station 2, which was sampled on all five cruises (Table 2). High frequency (30 min) salinity and temperature data from TABS Buoy B were averaged to daily values for the month of September in each year and were used to compare against buoy data from September 2017. In addition, historical Chl-*a* data were obtained from SEAMAP cruises over 6 years (2006, 2008–2009, 2015–2016, 2018; courtesy of G. Zapfe). Surface Chl-*a* data from Stations 1 to 7 collected in the months of September and October were used. The historical SEAMAP Chl-*a* data used a modified Welschmeyer method (1994) which does not use acidification in the analyses. To account for this, pre-acidification Chl-*a* concentrations measured in the analyses of the cruise-based samples (Parsons et al. 1984) were used for comparison to the historic dataset. With the exception of this comparison to SEAMAP data, all other Chl-*a* values reported in the current study are those with acidification step.

Statistical analyses

Statistical analyses were conducted using the "vegan" (version 3.6.1; Oksanen et al. 2019) and "Xnomial" (version 1.0.4; Engels 2015) packages in R (R Core Team 2016). Historical buoy salinity data were square root transformed to better approximate a normal distribution, while environmental and abundance data were transformed using natural log $(x + 1)$ to eliminate the impact of zeroes on the data distribution (Behrens 1997). To limit the effects of temporal pseudo-replication, a repeated measure ANOVA (RM-ANOVA) was used to analyze the post-storm salinity and temperature data relative to the long-term dataset (Hurlbert and White 1993). A Kruskal–Wallis test was applied to K_{dPAR} and N^2 coefficients to analyze the difference between months with nonnormal distribution (Mcdonald 2014). An exact test for multinomial (XNomial) was used to compare post hurricane (September and October 2017) total Chl-*a* biomass to the historical data set and to accommodate the small sample size and lack of true replication (Mcdonald 2014).

For multivariate analyses, a natural log $(x + 1)$ transformation was applied to functional group abundances and environmental data to minimize the impact of zero values. The Bray Curtis index (Bray and Curtis 1957) was used to build a compositional dissimilarity matrix based on abundances of the size- and pigment-based groups from flow cytometry (PC, PE, ANAN, and HNAN). Analyses of similarity (ANOSIM) were conducted to determine if the group-based assemblages varied significantly between sites and/or months (Clarke et al. 2006). Canonical correspondence analysis (CCA) was used to measure the relationship between multivariate environmental conditions and group-based community (PC, PE, ANAN, and HNAN) assemblage change. Biplot scores for constraining variables from the CCA analyses were used to quantify the contribution of each environmental factor to changes in the group-based assemblage structure (ter Braak 1986). Additionally, Spearman's rank correlation analyses were conducted to quantify monotonic relationships between individual group abundances (PC, PE, ANAN, and HNAN) and environmental factors (Supporting information Fig. S3).

Results

The physicochemical environment

Salinity and temperature data from Stations 2, 6, and 10 were available pre- (July 2017) and post-Hurricane Harvey (September 2017 to March 2018; Supporting information Fig. S1). Surface salinities at Stations 2 and 6 were greatly reduced in both September and October 2017 compared to salinity measured at the same locations in July 2017 (Supporting information Fig. S1). These reduced salinities are underscored by TABS Buoy B salinities measured in September 2017 (mean = 23.43, SD = 2.89) that were 29% lower than average salinities at the same location in the historic dataset (September 2013–2016, 2018; Fig. 2; RM-ANOVA, $F_{5,162} = 127.6$, $p < 0.05$). Surface temperatures measured on September and October 2017 cruises were also reduced when compared to July 2017 (Supporting information Fig. S1) and were 3.6% lower at TABS Buoy B in September 2017 compared to the historical dataset (Fig. 2; RM-ANOVA, $F_{5,162} = 28.91$, $p < 0.05$).

Water column stratification, represented as buoyancy frequency (N^2) varied over the study period and region (Kruskal Wallis, $p < 0.05$) along with changes in salinity and temperature (Fig. 3). Station 2 was well-mixed (lowest N^2) in July while more marked stratification (higher N^2) was observed at this and other nearshore stations, especially Stations 1 and 3, following Hurricane Harvey in September (Fig. 3). These stations

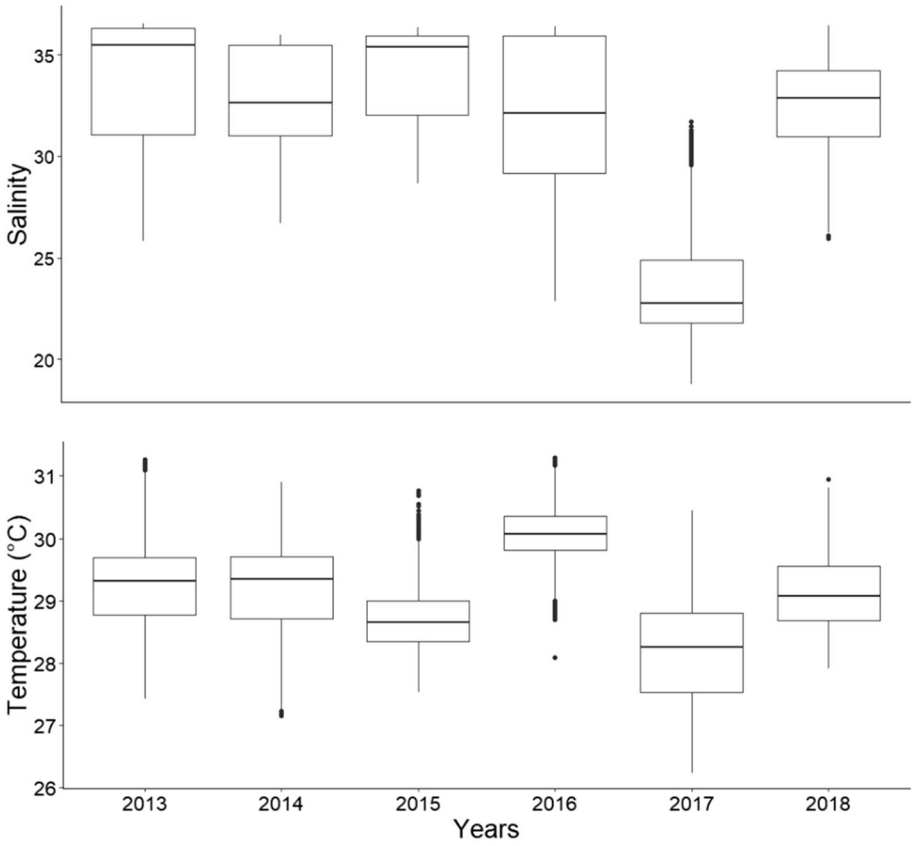

Fig. 2. Box-whisker plot of September salinity (top) and temperature (bottom) from 2013 to 2018 from the TABS Buoy B. Each box shows median, two hinges, and two whiskers. The lower and upper hinges correspond to the first and third quartiles (the 25th and 75th percentiles, respectively). Data beyond the end of the whiskers are outliers and are plotted individually.

transitioned back to more well-mixed conditions in October, with stratification increasing again in March 2018 (Fig. 3). In contrast, mid-shelf Station 6 was already stratified in July, with a strong thermocline and pycnocline below 20 m, and this stratification persisted through 30 m at this and other mid-shelf stations (i.e., 4–7) following Hurricane Harvey in September and October (Fig. 3; Supporting information Fig. S1). Offshore Station 10 was strongly stratified in July, driven mainly by warm, low salinity water at the surface (Fig. 3; Supporting information Fig. S1). All offshore stations show lower N^2 values in subsequent months (October, January, and March) compared to July (Fig. 3; Supporting information Fig. S1).

Maximal light attenuation coefficient values (K_{dPAR}; i.e., most rapid loss of light with depth) were measured at nearshore stations and decreased towards offshore stations with the exception of Station 2 (Fig. 3). January showed highest attenuation at nearshore Stations 1 and 2, suggesting highest suspended sediments/turbidity in this month. While October K_{dPAR} at Station 1 was relatively high compare to March, K_{dPAR} at Station 2 in October was minimal, suggesting a high degree of spatial variability. (Fig. 3, Supporting information Fig. S1). Mid-shelf and offshore regions showed less variability in October compared to March and January (Fig. 3, Supporting information Fig. S1). October values stayed lowest through the gradient between Stations 5 and 10 (Fig. 3). PAR (μmol photons m^{-2} s^{-1}) also showed an even distribution in the water column in October and high surface-deep differences in January at nearshore stations (Supporting information Fig. S1). However, attenuation coefficients did not show significant differences between months (Kruskal Wallis; $p > 0.05$) and CCA analyses did not indicate K_{dPAR} as a significant explanatory variable for community compositional changes.

Nearshore and mid-shelf stations had generally lower nutrient concentrations in October compared to the months following (January 2018–March 2018). It should be noted that nutrient samples were not collected in September and ammonium was not sampled in July. At Stations 2, 6, and 10, nitrate concentrations throughout the water column were higher in July 2017 than in any of the subsequent months (Supporting information Fig. S2). Surface nitrate concentrations at Station 2 were highest (0.10 μM) in July compared to October and subsequent cruises (< 0.04 μM; Supporting information Fig. S2). While surface nitrate also remained low at Stations 6 and 10, increased concentrations at depth were observed at these mid-shelf and offshore stations in October and January

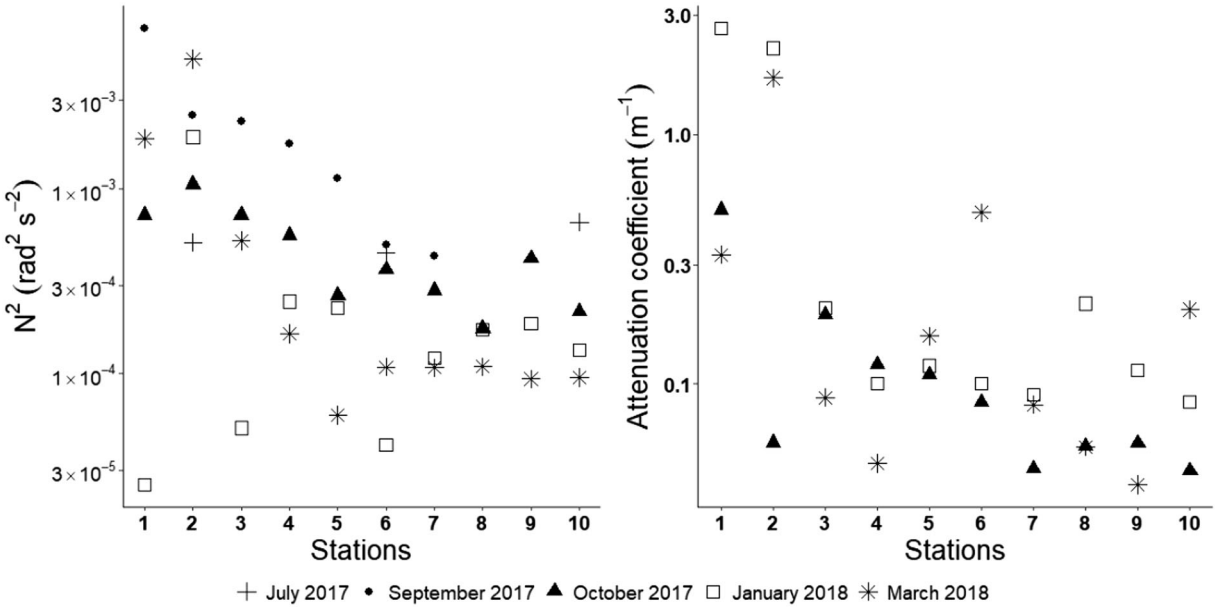

Fig. 3. Brunt-Väisälä frequency (N^2, rad^2 s^{-2}; left) and light attenuation coefficient (K_{dPAR}, m^{-1}; right) mean values for each station (x-axis) represented with symbols based on months: July 2017 (cross), September 2017 (circle), October 2018 (triangle), January 2018 (square), and March 2018 (star). For deeper, offshore stations, N^2 and attenuation coefficients were calculated for only the upper 150 m in the water column. *Note:* attenuation coefficients are not provided for July 2017 and September 2017 due to lack of PAR data.

(Supporting information Fig. S2). With the exception of January, Station 10 nitrate concentrations reached > 5.0 μM at depth (Supporting information Fig. S2). Silicate was also highest in July at Stations 2 and 10, both at the surface and at depth (Supporting information Fig. S2). Surface silicate concentrations were lower at Stations 2 (4.93 μM) and 10 (1.10 μM) in October compared to July (11.30 μM, 4.30 μM; Supporting information Fig. S2), while surface silicate concentrations in October at Station 6 were nearly twice the concentrations in July (3.08 μM; note scale of Supporting information Fig. S2).

In contrast, surface concentrations of phosphate were at their lowest at all stations in July compared to the post-storm months (Supporting information Fig. S2). At Stations 2 and 6, surface phosphate concentrations were lowest (0.10–0.26 μM) in July, showed higher concentrations (> 0.30 μM) in October, and remained at comparable levels in January and March (Supporting information Fig. S2). Surface concentrations of phosphate at Station 10 were lower in July compared to subsequent months (Supporting information Fig. S2). Maximum phosphate concentrations were observed at depth in October (0.72 μM) and March (0.85 μM; Supporting information Fig. S2). Across the stations, ammonium concentrations also showed their highest values in October (9.27 μM) and January (8.65 μM), compared to generally low concentrations in March (0.33 μM; Supporting information Fig. S2). However, there were no ammonium concentrations from July available for comparison.

Generally, the nutrient ratio data indicate DIN:Si ratios were below than Redfield ratio at nearshore and intermediate stations in March and Stations 1 and 2 in October and January (Supporting information Fig. S4), respectively, trends that can be best explained by very low nitrate concentrations in those water columns (*see* Supporting information Fig. S2). DIN:Si ratios generally increased from nearshore to offshore, largely due to increased subsurface nitrate concentrations at offshore stations (*see* Supporting information Figs. S2 and S4). Increasing ratios from nearshore to offshore were also pronounced in the DIN:DIP ratios, again seemingly due to increased subsurface nitrate concentrations at offshore stations (*see* Supporting information Figs. S2 and S4). DIN:DIP ratios were near or above Redfield ratio in October and January and below Redfield ratio in March. A notable exception is a greater Redfield than DIN:DIP ratio at Stations 1 and 4 in October (Supporting information Fig. S4).

Changes in phytoplankton biomass

Vertical CTD profiles showed higher Chl-*a* fluorescence throughout the water column at Stations 1 and 3 in September than in October; however, extreme surface values at Station 2 were notably higher in October than September (Supporting information Fig. S1). Chl-*a* fluorescence at mid-shelf stations showed generally comparable or lower biomass during this same period (Supporting information Fig. S1). Distinct subsurface Chl-*a* fluorescence maxima were common at mid-shelf stations in September (Supporting information Fig. S1) and at both mid-shelf and offshore stations in October and March (Supporting information Fig. S1). Subsurface Chl-*a* fluorescence maxima were largely absent in January, corresponding with generally less stratified water columns (as N^2 than in October (Fig. 3). CDOM fluorescence values

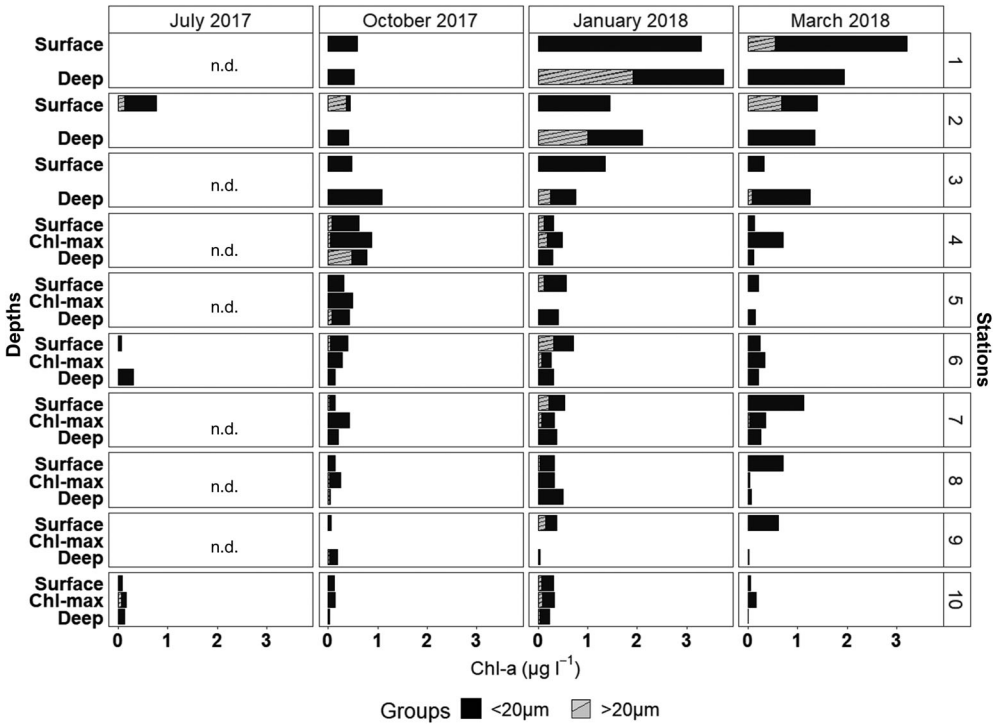

Fig. 4. Size-fractionated Chl-*a* (μg l^{-1}) biomass in the < 20 μm (black) and > 20 μm (stripe) size classes from Stations 1 to 10 from July 2017, October 2017, January 2018, and March 2018. Note that only three stations (2, 6, and 10) were sampled in July 2017, stations that were not sampled in that month are noted by "n.d."

were highest at all stations in January compared to October and March. Note that neither CDOM nor Chl-*a* fluorescence data were collected in July, and only nearshore and shelf stations have Chl-*a* fluorescence data in September.

Beyond changes in overall Chl-*a* in the months following Hurricane Harvey derived from fluorescence, the distribution of extracted Chl-*a*, both in total and resolved across two size-classes of phytoplankton, also showed distinct changes. Generally, biomass decreased from nearshore to offshore stations, and changes in size-fractionated Chl-*a* during the study period were less apparent at mid-shelf or offshore stations (Fig. 4). An exception is in October, when maximum biomass dominated by the smaller < 20 μm size class was observed at Stations 3 and 4 (vs. nearshore or further offshore stations; Fig. 4). Biomass at mid-shelf and offshore stations was generally dominated by the smaller < 20 μm size class. However, the larger microphytoplankton (> 20 μm) contributed more to overall biomass across several stations in January (Fig. 4).

Total Chl-*a* decreased from July (0.77 μg l^{-1}) to October 2017 (0.44 μg l^{-1}) at Station 2, most of which can be attributed to a 90% decrease in biomass of the smaller pico- and nanoplankton size class (< 20 μm; Fig. 4). Overall, Chl-*a* biomass increased at Station 2 in both January and March 2018 (Fig. 4) primarily due to increases in microphytoplankton (> 20 μm) biomass at depth in January and at the surface in March (Fig. 4). Similar shifts in depth-specific phytoplankton size structure in January and March 2018 were also observed at Station 1 (Fig. 4). At mid-shelf Station 6, the < 20 μm size class dominated biomass in July and October 2017 and < 20 μm biomass at the surface was higher in October compared to July (Fig. 4). In contrast, October < 20 μm biomass were lower than July at deep samples (Fig. 4). Chl-*a*

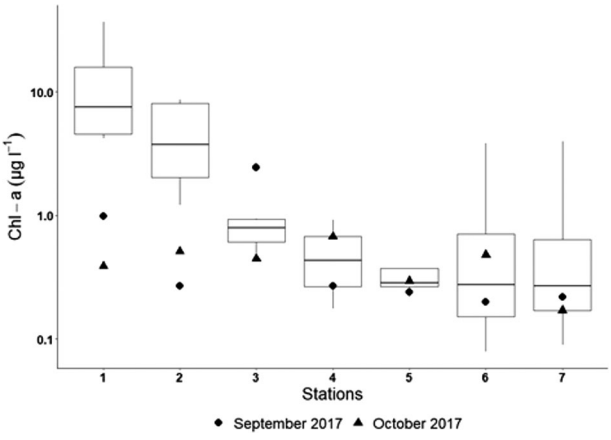

Fig. 5. Box-whisker plot of fall (September and October) surface Chl-*a* (μg l^{-1}) samples from 2006, 2008–2009, 2015–2016, and 2018 SEAMAP cruises from Stations 1 to 7. Each box shows median, two hinges, and two whiskers. The lower and upper hinges correspond to the first and third quartiles (the 25th and 75th percentiles, respectively). Points indicate midpoint of surface Chl-*a* (μg l^{-1}) duplicate measurements from September (circle) and October 2017 (triangle).

biomass remained low (< 0.71 $\mu g\, l^{-1}$) at the offshore stations throughout the study period, and size-fractionated biomass at Station 10 showed little change from July 2017 through March 2018 (Fig. 4).

To determine if changes in overall phytoplankton biomass following Hurricane Harvey differed from expectations of interannual variability in the study region, surface Chl-*a* measured from Stations 1 to 7 in September and October 2017 were compared to surface Chl-*a* concentrations measured on fall SEAMAP cruises (September, October) from 6 years for which data were available (2006, 2008–2009, 2015–2016, 2018). Post-storm Chl-*a* biomass at Stations 1 and 2 was an order of magnitude lower than median Chl-*a* from the historical dataset (XNomial, $p < 0.05$; Fig. 5); however, post-storm biomass at Stations 3–7 were not significantly different from the historical dataset (Fig. 5).

Changes in pico- and nanoplankton abundances

Within the pico- (0.2–2 μm) and nanoplankton (2–20 μm), which generally dominated Chl-*a* biomass (i.e., the < 20 μm size fraction), we resolved changes in abundance of four main functional groups: picoeukaryotes (PE), picocyanobacteria (PC), heterotrophic nanoplankton (HNAN), and autotrophic nanoplankton (ANAN). Mixotrophic plankton were not distinguished from ANAN due to an inability to quantify mixotrophy in the field (i.e., Carvalho and Granéli 2006). Overall, abundances of these functional groups decreased from nearshore (Fig. 6, top plots) to offshore (Fig. 6, bottom

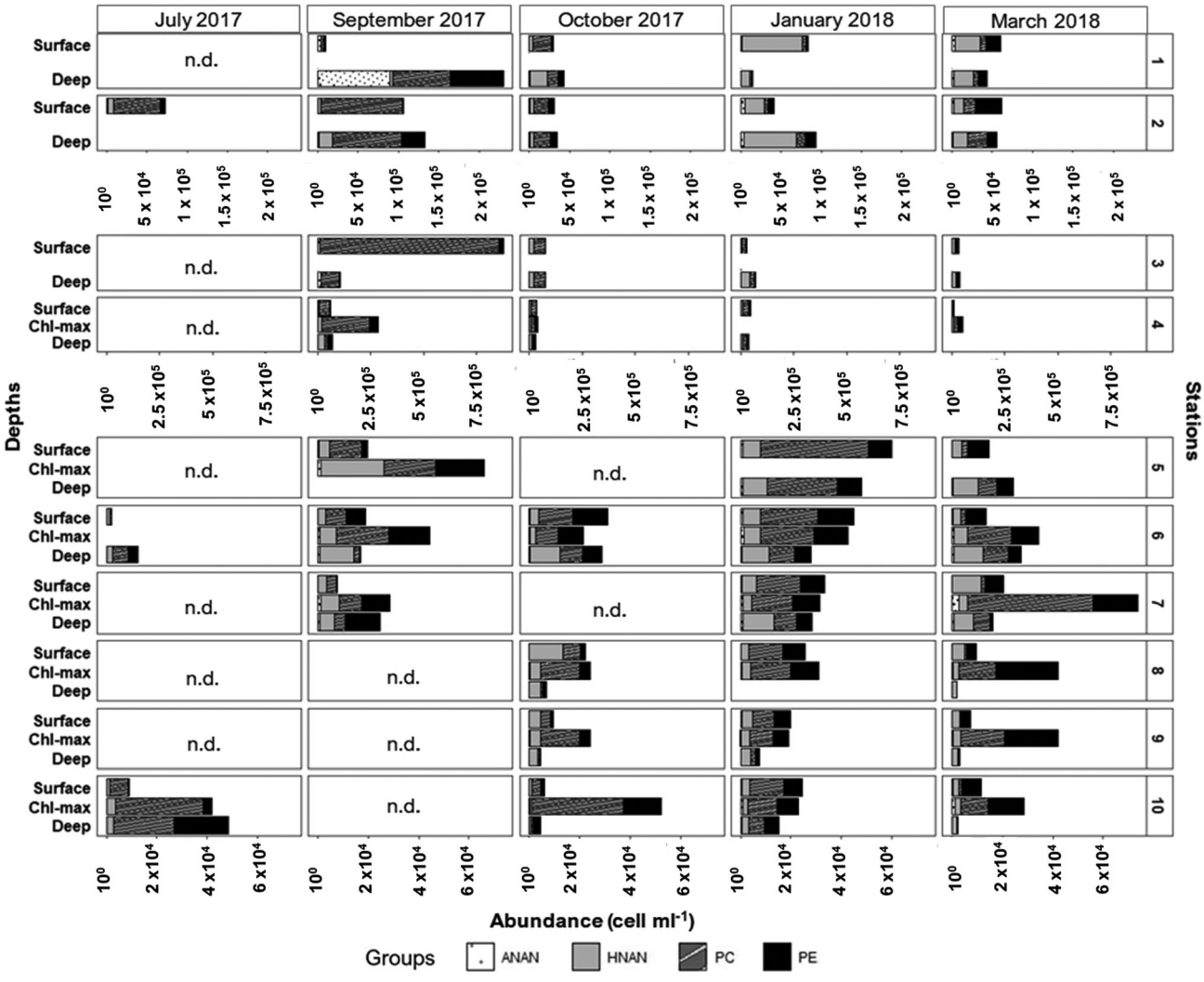

Fig. 6. Abundances of functional groups autotrophic nanoplankton (ANAN), heterotrophic nanoplankton (HNAN), picocyanobacteria (PC), and picoeukaryotes (PE) from Stations 1–2 (top rows), 3–4 (middle rows), and 5–10 (bottom rows). Data are presented from July 2017, September 2017, October 2017, January 2018 and March 2018, but note that some stations were not sampled in July or September and samples from stations 5 and 7 in October 2017 were lost (noted by "n.d."). Note that the different axis limits were used in each grouping of graphs to allow for the full range of data to be visualized.

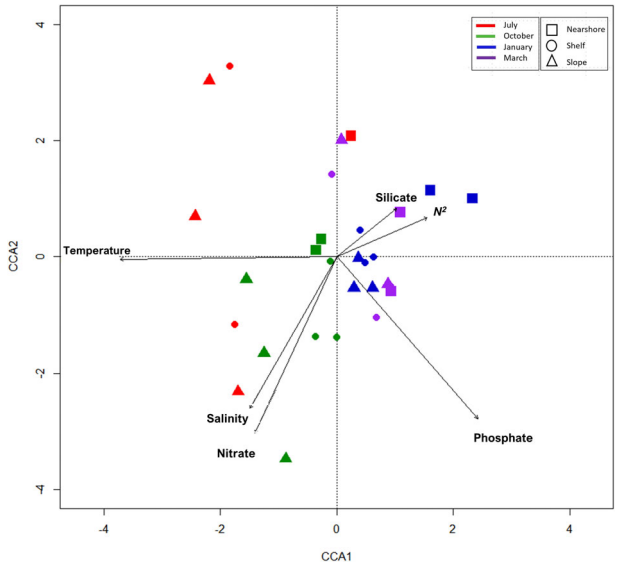

Fig. 7. CCA ordination of group-based pico- and nanoplankton assemblage and explanatory environmental variables. Figure includes assemblage and variable data from nearshore (Station 2, square), shelf (Station 6, triangle), and offshore (Station 10, circle) only, in July 2017 (red), October 2017 (green), January (blue), and March 2018 (purple). Note that the data from the deep Station 10 sample in March was excluded from the analyses due to off-scale ordination, primarily driven by an especially high nitrate value.

plots; note different axis limits), a trend that is similar to that observed for overall and size-fractionated Chl-*a* biomass (Fig. 4). One exception was Station 3 in September, where surface abundances of PC (8.4×10^5 cells ml^{-1}) and PE (2.5×10^4 cells ml^{-1}) were higher than abundances at any other station or timepoint (Fig. 6). Generally, pico- and nanoplankton abundances at each station were lower in October than in other months sampled, with exceptions in the Chl-*a* max at offshore stations (Stations 8–10; Fig. 6, bottom plots). For the three stations sampled in July (Stations 2, 6, and 10), the pico- and nanoplankton abundances showed contrasting patterns in September and October. At Station 2, specifically, PC abundances were 69% higher in September compared to July, followed by subsequently lower abundances in all pico- and nanoplankton groups in October (Fig. 6). HNAN abundances were tenfold higher in January 2018 than October 2017 and dominated the pico- and nanoplankton assemblage in January 2018, while the pico- and nanoplankton assemblage was more evenly distributed among the groups in March 2018 (Fig. 6, top plots).

At mid-shelf Station 6, higher pico- and nanoplankton abundances were observed at all depths during September and October 2017 compared to July 2017 (Fig. 6, bottom plots; note that Chl-max was not sampled in July). The September 2017 assemblages were dominated by PC (1.6×10^4 cells ml^{-1}) and PE (2.0×10^4 cells ml^{-1}) in the Chl-max samples, and HNAN (1.3×10^4 cells ml^{-1}) in the deep samples (Fig. 6, bottom plots). More even distribution among groups was observed in October (Fig. 6, bottom plots). Pico- and nanoplankton abundances were maximal at Station 6 in January 2018, driven primarily by PC and PE in surface and Chl-max communities and HNAN at depth. Lower abundances in Station 6 surface waters were observed in March 2018 (Fig. 6, bottom plots). Offshore at Station 10, surface communities were generally dominated by PC, and already low abundances in July were further reduced in October (Fig. 6, bottom plots). Samples were not collected at Station 10 in September (Table 2). Abundances of picoplankton in the

Table 3. Results of canonical correlation analyses of group-based pico- and nanoplankton assemblage and environmental variables from Stations 2, 6, and 10 in July and October 2017, and January and March 2018 (pre- and post-hurricane) and all stations in October 2017, January and March 2018 (post-hurricane only). Table presents constrained and unconstrained inertia proportion ranks of CCA test, biplot scores for constraining explanatory environmental variables of CCA plot (CCA1), and *p* value for each variable.

	Pre- and post-hurricane		Post-hurricane only	
Constrained	63%		44%	
Unconstrained	37%		56%	
Variables	CCA1 scores	*p* value	CCA1 scores	*p* value
Temperature	−0.90	0.001*	−0.20	0.004*
Salinity	−0.36	0.071	−0.35	0.015*
Stratification (N^2) coefficient	0.38	0.631	0.30	0.132
Nitrate	−0.34	0.019*	−0.70	0.001*
Phosphate	0.59	0.007*	−0.88	0.001*
Silicate	0.25	0.819	−0.04	0.746
Ammonium	n.d.	n.d.	−0.07	0.817
CDOM	n.d.	n.d.	0.49	0.028*
Attenuation coefficient (K_{dPAR})	n.d.	n.d.	0.39	0.439

*Significant predictor variables ($p < 0.05$).

Chl-max at Station 10 increased in October, most notably PE abundances which were 76% higher in October than July 2017 (Fig. 6, bottom plots). Surface and deep abundances at Station 10 were higher in January 2018, with more even distribution among groups. A distinct Chl-max was again dominated by PC and PE in March 2018 (Fig. 6, bottom plots).

Changes in nano- and picoplankton abundances at Stations 2, 6, and 10 from July 2017, October 2017, January 2018, and March 2018 ($n = 32$) resulted in distinct group-based assemblage structure according to month (ANOSIM, $p < 0.05$, R: 0.15) but not station (ANOSIM, $p > 0.05$, R: 0.08). Results of the CCA further indicate that environmental factors explained 63% of the variance (constrained proportion) in the overall pico- and nanoplankton group-based assemblages from pre- and post-storm stations (Fig. 7; Table 3). Nitrate and temperature were significant and negatively correlated predictor variables, while phosphate was a significant and positively correlated predictor variable of group-based assemblages across (Table 3). Note that the Station 10 deep sample in March was excluded from CCA analyses due to off-scale ordination, primarily driven by an especially high nitrate value. When all 10 stations from only post-hurricane months (October 2017, January 2018, and March 2018) were analyzed ($n = 66$), pico- and nanoplankton group-based assemblages also showed significant differences based on month (ANOSIM, $p < 0.05$, R: 0.05) and across stations (ANOSIM, $p < 0.05$, R: 0.12). In this larger analysis, phosphate, salinity, nitrate, temperature, and CDOM were significant explanatory variables (44% of the variance, constrained proportion) in the group-based, post-storm assemblages (Table 3). The R values for both ANOSIM analyses are quite low, however, and so these results should be interpreted with caution. However, when correlations between individual group abundances with environmental factors are considered, ANAN, HNAN, and PC abundances post-storm are all negatively correlated with salinity but positively correlated with attenuation coefficient (K_{dPAR}; Supporting information Fig. S3). Interestingly, PE abundances were not significantly correlated with any environmental variables in the dataset, while PC showed a negative correlation with nitrate concentrations (Supporting information Fig. S3). Pre- and post-hurricane data showed negative correlations with temperature and salinity on both ANAN and HNAN abundances.

Discussion

This study contributes to our understanding of post-storm environments and responses of small plankton by quantifying the influence of Hurricane Harvey on the smallest members of plankton communities and at larger scales ranging from the mouth of Galveston Bay to the GOM basin in the weeks and months following the storm. As such, this study complements the numerous studies conducted in Galveston Bay following Hurricane Harvey that provide information about the immediate responses of the bay's ecosystem in the month following the storm (e.g., Du et al. 2019a, Steichen et al. 2020, Yan et al. 2020; and others). These studies show that an influx of freshwater from Hurricane Harvey caused low salinity conditions that extended to the outside of Galveston Bay (Du et al. 2019a), conditions that correspond with decreased surface salinities at the nearshore stations in our study (stations 1–3) relative to 5-year median values from the TABS buoy system (Fig. 2, Supporting information Fig. S1). Within the 3 weeks following Hurricane Harvey, nitrate concentrations increased throughout Galveston Bay, and stations in the upper bay continued to increase throughout the rest of the month (up to 40 μM) while concentrations at the mouth and outside of the bay started to decrease after 4 weeks (to 0.79 μM; Steichen et al. 2020). Similarly, phosphate concentrations increased throughout the month (up to 4.46 μM) in the upper bay and started to decrease outside of the bay after 1 month (to 2.63 μm; Steichen et al. 2020). These results correspond with the very low nitrogen (< 0.04 μM) and phosphate concentrations (< 0.55 μM) we observed at surface nearshore stations in October (Supporting information Fig. S2).

Along with the freshwater and nutrients, terrigenous dissolved organic carbon (tDOC) and bacteria were exported to the continental shelf through the end of September (D'Sa et al. 2018, Steichen et al. 2020). Within Galveston Bay, estuarine-marine prokaryotic species were replaced with terrestrially derived heterotrophic microbial species and freshwater phytoplankton groups dominated primary producer communities 2 weeks following the hurricane (Steichen et al. 2020). High microbial activity was observed within the bay as a response to increase tDOC input, and bacterial removal of $\sim$ 70% of the tDOC, resulted in alterations of net CO_2 exchange and nutrient budgets in the area (Yan et al. 2020). Two months following the storm, more marine-derived haptophytes and prochlorophyte groups increased their relative abundance at the Galveston bay (Liu et al. 2019). During that same period, phytoplankton PSII photochemical efficiency (Fv/Fm) was maximal in the mid-bay and low in more nutrient-limited adjacent shelf waters (Liu et al. 2019), conditions that correspond with the reductions in surface biomass at Station 2 from July to October (Fig. 4) and low group-based abundances at Station 1 in September (Fig. 6) in the current study. This study thus expands our understanding of the impacts of Hurricane Harvey outside of the bay, for an extended period from 3 weeks to several months post-event, and with specific focus on the critical, smallest members of pelagic communities, the pico- and nanoplankton.

Nearshore environment

Our results extend the understanding of the spatial and temporal scale of hurricane impacts on plankton community dynamics onto the continental shelf and in the months following the storm. Inorganic nutrient concentrations at nearshore continental shelf station, especially nitrate were lower 2 months following the storm when compared to pre-storm

(July 2017) and later timepoints (January and March 2018; Supporting information Figs. S2 and S4). Silicate concentrations at Station 1 (< 10 μM) complement to observations by Steichen et al. (2020) of reductions in surface silicate (from 51 to 30 μM in the 5 weeks after Hurricane Harvey) at the mouth of Galveston Bay. That study also documented sequential blooms of diatoms followed by dinoflagellates at the estuary mouth (Steichen et al. 2020), a region that is close to our nearshore Station 1. DIN:DIP ratios were same level in October with Redfield ratio at nearshore region, but they were higher compared to March (Supporting information Fig. S4). Our results, from the nearshore waters just beyond Galveston Bay to the offshore waters of the continental slope, do not show any evidence for a bloom or increased biomass in the 3–8 weeks after Hurricane Harvey. Rather, total phytoplankton biomass (as Chl-*a*) in surface, nearshore waters was significantly lower in September/October 2017 than any measurements from a 6-year historical dataset in those months (Fig. 5). These results do correspond with the findings of Liu et al. (2019), which documented decreases in the high Chl-*a* concentrations outside of the bay (close to our Station 1) after 2 months post-storm. Taken together, results from our research and previous studies (Liu et al. 2019; Steichen et al. 2020) suggest that, while depleted nutrient concentrations may indicate a post-bloom environment in our nearshore stations prior to our sampling, increased phytoplankton biomass was largely restricted in space and time to the estuarine waters of Galveston Bay and/or to the initial month following Hurricane Harvey.

The reductions in Chl-*a* biomass that we observed post-storm in nearshore waters are in contrast to previous studies which have shown increased phytoplankton biomass post-storm (e.g., Walker et al. 2005, Merritt-Takeuchi & Chiao 2013) and observations of increased Chl-*a* in the Mission-Copano Bay estuary in the 2–3 months following Hurricane Harvey (Patrick et al. 2020). However, our results agree with three studies that reported no change or reductions in biomass following tropical cyclones (Chang et al. 1996; Wetz and Paerl 2008a, Paerl et al. 2020). Wetz and Paerl (2008a) emphasized the importance of water column stratification prior to storm events in shaping the response of phytoplankton after a tropical cyclone. More specifically, Chl-*a* decreased or showed no change after a storm when the pre-storm water column was already well-mixed, whereas stratification pre-storm was associated with post-storm increases in biomass (Wetz and Paerl 2008a). Nearshore stations in July 2017 were generally well-mixed, as evidenced by vertical profiles (Supporting information Fig. S1) and the lowest Brunt–Väisälä buoyance frequency (N^2) measured at Station 2 in the study (Fig. 3). The decreased biomass we observed at Station 2 in the 3 weeks and 2 months following Hurricane Harvey therefore fits with the expectations for well-mixed water columns, based on Wetz and Paerl (2008a). Furthermore, this dependence of phytoplankton response to a large tropical cyclone on antecedent physical conditions underscores the need to characterize pre-storm conditions to better predict and understand post-storm effects (Hogan et al. 2020).

Significantly lower Chl-*a* biomass in September and October compared to previous years in the same months and at the same nearshore stations (Fig. 5) strongly suggests that these results are tied to the hurricane effects and not just seasonal cycles or trends in biomass. These observed reductions in phytoplankton biomass were primarily due to reductions in phytoplankton biomass in the < 20 μm size-fraction in October throughout the study system (Fig. 4). Picocyanobacteria were also reported to decrease (from an average of 20%–30% to < 5%) in Galveston Bay in the week following Hurricane Harvey, followed by an increase over the next 4 weeks in the outer bay (Steichen et al. 2020). These results align with high abundances of picocyanobacteria that we observed in nearshore stations in September 2017, 3 weeks following the storm (Fig. 6). Our study followed such changes further out onto the shelf and into the following months, revealing continued low abundances of pico- and nanoplankton at Stations 1 and 2 into October 2017 (Fig. 6). The nearshore picoplankton abundances we observed in October 2017 (10^4 to 5×10^4 cells ml^{-1}), specifically, were lower than those measured at the mouth of Galveston Bay (10^6 cells ml^{-1}; Williams and Quigg 2019) and the broader nGOM shelf region (7.1×10^4 cells ml^{-1}; Williams et al. 2015). These results also correspond with 100%-fold decrease of picophytoplankton abundance that Paerl et al. (2020) observed following Hurricane Florence in the Neuse River Estuary. That study highlighted the importance of precipitation as a factor on pico- phytoplankton abundance and composition (Paerl et al. 2020) which was one of the main influences of Hurricane Harvey. A second important factor that both Chang et al. (1996) and Paerl et al. (2020) pointed out is the impact of temperature on these groups. Our study also shows reduced temperatures in the aftermath of Hurricane Harvey and a negative correlation between temperature and ANAN and HNAN abundances (Supporting information Fig. S3). Together, these results build a deeper understanding of the physical constraints of reduced salinity and temperature on pico- and nanoplankton growth following extreme precipitation and/or tropical cyclone events.

Our results suggest that the large influx of nutrients delivered to the continental shelf via floodwaters in the immediate aftermath of Hurricane Harvey (D'Sa et al. 2018; Du et al., 2019b; Steichen et al. 2020) may have already been consumed by increased phytoplankton and/or bacterioplankton by the time of our October samples (Liu et al. 2019; Yan et al. 2020). The increase in picocyanobacteria (Fig. 6) and marine heterotrophic bacteria (Steichen et al. 2020) in September, followed by decreased abundances of these small picoplankton with high nutrient affinities (Joint et al. 2002) 2 months following the storm are likely explained by changes in the availability and/or exhaustion of macronutrients, especially nitrate and silicate. This interpretation of nutrient limitation explaining shifts in the pico- and nanoplankton assemblage is supported by the CCA

results, in which both nitrate and phosphate were significant predictor variables (Fig. 7, Table 3). More specifically, shifts in abundance with nutrients are also supported by negative correlation of nitrate with both HNAN and PC abundances and negative correlation of phosphate with ANAN abundances (Supporting information Fig. S3). Our data therefore suggest that the inverse relationships of nitrate from the CCA results may be explained by significant uptake of these nutrients, especially by picoplankton and/or heterotrophic bacterioplankton, at the same time or preceding our sampling timepoints. Results from Liu et al. (2019) and Steichen et al. (2020) further suggest that short-term responses of increased biomass in larger plankton groups (e.g., diatoms, dinoflagellates, etc.) within Galveston Bay may explain the relative nutrient scarcity, especially in nitrate, that we observed in October.

Finally, active benthic phytoplankton communities in the nearshore waters could also have resulted in drawdown of nutrients in the 2 months between the storm and our first nutrient samples (late October 2017). The Texas continental shelf is characterized by a mix of pelagic and benthic phytoplankton communities during June and July and a net primary production done by nepheloid layer (Kamykowski & Bird 1981). However, this benthic contribution to primary production has been shown to weaken in September and other fall months (Kamykowski & Bird 1981), so it is possible that benthic primary production in the 6 weeks following Hurricane Harvey was less of a contribution than during other times of year. Finally, it is also possible that availability of micronutrients such as iron (Botebol et al. 2017), cobalt, or manganese (Ahlgren et al. 2014) also played a role in changing communities in the aftermath of Hurricane Harvey. More in-depth biogeochemical analyses, integration of both pelagic and benthic biomass measures, and more finely resolved timeseries data that resolve both pre- and post-storm nutrient regimes, are required to elucidate these potential alternative hypotheses.

The potential for light limitation of phytoplankton biomass and shifts in community structure was also investigated in our dataset. High tDOC and sediment load caused high turbidity in Galveston Bay (https://visibleearth.nasa.gov/images/90866/texas-waters-run-brown-after-harvey), which could lead to increased light attenuation and light-limitation in coastal waters (Peierls et al. 2003). Chl-*a* concentrations in the bay increased three-fold in the 2 weeks following the hurricane and stayed higher than any measurements from the prior year (10 $\mu g\, l^{-1}$; Liu et al. 2019). This increase in phytoplankton biomass suggests that increased sediment load and turbidity in the bay, at least, was not limiting production in the weeks immediately following the storm. Outside of the bay, CDOM concentrations started to dissipate 2 weeks following the storm (D'Sa et al. 2018), and our data show low attenuation coefficients (K_{dPAR}; i.e., higher light penetration to depth) at nearshore stations in October (Fig. 3; Supporting information Fig. S1). CCA analyses that included K_{dPAR} did not indicate light attenuation as a significant explanatory variable in functional group composition (Table 3). Together, these results suggest that the direct effects of increased sediment load on the nearshore water column were largely over within 6 weeks post-storm and that changes in biomass and pico- and nanoplankton abundances that we observed in the aftermath of Hurricane Harvey are not explained by changes in the underwater light field.

CCA results do, however, indicate correlations of physical signals from Hurricane Harvey (i.e., temperature, salinity, and CDOM) with the observed changes in the pico- and nanoplankton assemblage (Table 3). The importance of temperature in structuring the pico- and nanoplankton community has been observed in other studies, for example as decreased *Synechococcus* (Chang et al. 1996) and PC abundances (Paerl et al. 2020) linked to reduced water temperatures following storms. Our results showed a significant reduction in nearshore surface temperatures post-storm, both in the September and October CTD data (Supporting information Fig. S1). The September water temperature decrease is significantly lower than median temperature for that month in a 5-year buoy dataset (Fig. 2) and therefore may be attributable to Hurricane Harvey. The observed decrease in October water temperature, however, may reflect seasonal trends. Only ANAN and HNAN were negatively correlated with temperature in the bivariate comparisons (Supporting information Fig. S3). This inconsistency between the bi- vs. multivariate analyses emphasizes the need to understand both group-specific and assemblage-level changes in the context of the many factors that can limit growth and change competitive outcomes.

Additionally, attribution of changes in phytoplankton biomass or assemblage to changes in purely bottom-up or environmental controls following a tropical cyclone may underestimate the potential for changes in grazer communities and grazing activity following such events. Increases in microzooplankton numbers (Wetz and Paerl 2008b) and time-lagged grazing rates (Morison et al. 2019) have been documented in the aftermath of storms, and recent study indicates increased mesozooplankton abundances in the nearshore waters of our study region following Hurricane Harvey (Topor et al. 2020). Both microzooplankton and copepod grazing rates were quantified in October, January, and March during the same cruises and in the broader region prior to Hurricane Harvey in July, and these findings will be discussed in forthcoming papers. This article does resolve HNAN population dynamics, and more specifically shows high HNAN abundances in January and low HNAN abundances in September and October at Stations 1 and 2 (Fig. 6). These protistan consumers are known to represent significant sources of marine bacterioplankton mortality (including picocyanobacteria; Strom 2000), so it is possible that low HNAN abundance in September may have allowed for the increased PC abundances observed in that month (Fig. 6). It is also possible that other grazer groups (e.g., microzooplankton) or sources of mortality

(e.g., viruses) were factors in the observed changes in pico- and nanoplankton group abundances.

Mid-shelf environment

Changes in the physicochemical environment, together with pico- and nanoplankton biomass and assemblages, were also apparent in the mid-shelf region. At the mid-shelf station for which July data is available (Station 6), Chl-*a* increased in October (Fig. 4); however, the observed Chl-*a* concentrations in October were comparable to those measured in the historical dataset (Fig. 5). Effects of freshwater input were observed as reduced salinity in surface waters at Station 6 in September 2017 compared to just 1 month earlier, and surface salinities < 36 were measured throughout the mid-shelf stations in that month (Supporting information Fig. S1). However, decreased surface salinities and lower DIN:Si ratios were only observed at Stations 4 and 5, the most nearshore of the mid-shelf stations (56–88 km from shore) in October 2017. This indicates an alleviation of floodwater impacts 2 months after Hurricane Harvey at stations < 95 km offshore.

Biomass and abundances of pico- and nanoplankton at Station 6 in the mid-shelf region were substantially higher in September and October 2017 than in July 2017 (Fig. 6). In contrast to the nearshore pre-storm environment, the water column at Station 6 in July 2017 was stratified, as evidenced by a strong thermocline (Supporting information, Fig. S1) and relatively higher N^2 (Fig. 3). The observed increases in pico- and nanoplankton biomass and abundance in the 2 months following the storm thus also fit with expectations for enhanced phytoplankton biomass when a tropical cyclone induces mixing in a stratified water column (Wetz and Paerl 2008a, see more in-depth discussion above). While these changes in the pico- and nanoplankton assemblages appeared attributable to increases in picocyanobacteria and picoeukaryotes (Fig. 6), phytoplankton in the > 20 μm size-fraction also became important components of the overall biomass, especially in January 2018 (Fig. 4). This increase in larger biomass coincides with the highest surface silicate concentrations measured in this study (Supporting information Fig. S2), suggesting potential biogeochemical drivers for these changes further out from the coast and in time. Taken as a whole, our results suggest that, in mid-shelf waters, the effects of Hurricane Harvey may have led to initial increases in overall abundance of pico- and nanoplankton, but that these effects were not as long-lasting (< 2 months) as they were in more nearshore waters.

Offshore environment

Our results showed no discernible influence of the Hurricane Harvey-derived freshwater plume further offshore (> 150 km). Reduced surface salinities observed at Station 10 in late July 2017 (Supporting information Fig. S1) most likely represent the influence of the Mississippi River plume during that period (López-Veneroni et al. 1994; Du et al. 2019a). Offshore stations had DIN:Si ratios were higher than the Redfield ratio throughout the study (Supporting information Fig. S4). Overall phytoplankton biomass was generally low at Station 10 during the study period (max: 0.33 $\mu g\, l^{-1}$) and dominated by cells < 20 μm in size, consistent with previous studies from offshore Louisiana–Texas (Chakraborty and Lohrenz 2015; Gomez et al. 2018). Overall trends in offshore waters appeared to be more tied to seasonal cycles, with higher pico- and nanoplankton biomass in January, likely the result of a deepening mixed layer during that time (Chakraborty and Lohrenz 2015). Station 10 was not sampled in September, so it is difficult to know if any changes in nano- and picoplankton biomass or assemblage occurred in the period between Hurricane Harvey and the October cruise. However, based on the results available from this study, the three offshore stations we sampled appeared to be far enough from the discharge-driven impacts of Hurricane Harvey on the coastal ocean and are, instead, more related to changes in mesoscale ocean circulations (Biggs et al. 2005; Williams et al. 2015). Circulation-induced upwelling may have influenced offshore waters (Xu et al. 2017), but we were unlikely to see those effects without sampling closer to the event itself (i.e., in the days, not months, following storm passage).

Conclusions

Phytoplankton biomass and pico- and nanoplankton assemblages showed distinct changes across the Texas–Louisiana shelf in the weeks and months following Hurricane Harvey. We observed changes in salinity, temperature, and overall Chl-*a* biomass following Hurricane Harvey that were distinct from the pre-storm conditions and outside of the ranges of these variables in retrospective historical data analyses. Altered physicochemical conditions were associated with low phytoplankton biomass and pico- and nanoplankton abundances in nearshore waters, while direct effects on biomass and assemblages were less apparent in mid-shelf and largely lacking in the offshore waters of the continental slope. Pre-storm conditions in nearshore and mid-shelf waters were correlated with different phytoplankton responses to same hurricane and fit with expectations from stratified vs. well-mixed pre-storm water columns put forth by Wetz and Paerl (2008a). These variable responses, among stations within 50 km of each other, further underscore the need for better incorporating antecedent conditions into ongoing research on the ecosystem effects of extreme events (Hogan et al. 2020). This is the first study to report on the effects of tropical cyclone events on pico-and nanoplankton populations in the nGOM that extends beyond the estuarine environment to encompasses nearshore to offshore oceanic provinces for which long-term datasets (including pre- and post-storm sampling data) are rarely available. Our results suggest that the effects of an extreme event such as Hurricane Harvey can last at least 2 months in the nearshore waters of the continental shelf, where they can induce changes in both biomass and community composition of important plankton groups, size structure, and taxa. Given the importance of these smallest

members of the plankton as primary producers and primary consumers within the marine microbial food web, the effects of storm-induced changes in biomass and assemblages have important implications for ecosystem function in the region (Friedland et al. 2012).

References

Ackerman, J. D., L. R. Walker, F. N. Scatena, and J. Wunderle. 1991. Ecological effects of hurricanes. Bull. Ecol. Soc. Am. **72**: 178–180.

Ahlgren, N. A., A. Noble, A. P. Patton, and others. 2014. The unique trace metal and mixed layer conditions of the Costa Rica upwelling dome support a distinct and dense community of Synechococcus. Limnol. Oceanogr. **59**: 2166–2184. doi:10.4319/lo.2014.59.6.2166

Anglès, S., A. Jordi, and L. Campbell. 2015. Responses of the coastal phytoplankton community to tropical cyclones revealed by high-frequency imaging flow cytometry. Limnol. Oceanogr. **60**: 1562–1576. doi:10.1002/lno.10117

Babin, S. M., J. A. Carton, T. D. Dickey, and J. D. Wiggert. 2004. Satellite evidence of hurricane-induced phytoplankton blooms in an oceanic desert. J. Geophys. Res. Oceans **109**: C03043. doi:10.1029/2003JC001938

Barbero, L., D. Pierrot, R. Wanninkhof, and others. 2019. Third Gulf of Mexico ecosystems and carbon cycle (GOMECC-3) Cruise. doi: 10.25923/y6m9-fy08

Behrens, J. T. 1997. Principles and procedures of exploratory data analysis. Psychol Methods **2**: 131–160. doi:10.1037/1082-989X.2.2.131

Biggs, D. C., A. E. Jochens, M. K. Howard, S. F. DiMarco, K. D. Mullin, R. R. Leben, F. E. Muller-Karger, and C. Hu. 2005. Eddy forced variations in on- and off-margin summertime circulation along the 1000-m isobath of the northern Gulf of Mexico, 2000-2003, and links with sperm whale distributions along the middle slope. Geophys. Monogr. Ser. **161**: 71–85.

Blake, E. S., and D. A. Zelinsky. 2018. Hurricane Harvey. (AL092017). (AL092017) NOAA.

Botebol, H., G. Lelandais, C. Six, and others. 2017. Acclimation of a low iron adapted Ostreococcus strain to iron limitation through cell biomass lowering. Sci. Rep. **7**: 327. doi:10.1038/s41598-017-00216-6

Bray, J. R., and J. T. Curtis. 1957. An ordination of the upland forest communities of southern Wisconsin. Ecol. Monogr. **27**: 326–349. doi:10.2307/1942268

Campbell, L. 2001. Flow cytometric analysis of autotrophic picoplankton. Methods Microbiol. **30**: 317–343. doi:10.1016/S0580-9517(01)30051-X

Carvalho, W. F., and E. Granéli. 2006. Acidotropic probes and flow cytometry: A powerful combination for detecting phagotrophy in mixotrophic and heterotrophic protists. Aquat. Microb. Ecol. **44**: 85–96. doi:10.3354/ame044085

Chakraborty, S., and S. Lohrenz. 2015. Phytoplankton community structure in the river-influenced continental margin of the northern Gulf of Mexico. Mar. Ecol. Prog. Ser. **521**: 31–47. doi:10.3354/meps11107

Chang, J., C. Chung, and G. Gong. 1996. Influences of cyclones on chlorophyll a concentration and Synechococcus abundance in a subtropical western Pacific coastal ecosystem. Mar. Ecol. Prog. Ser. **140**: 199–205. doi:10.3354/meps140199

Christaki, U., C. Courties, R. Massana, P. Catala, P. Lebaron, J. M. Gasol, and M. V. Zubkov. 2011. Optimized routine flow cytometric enumeration of heterotrophic flagellates using SYBR Green I: FC analysis of HF. Limnol. Oceanogr. Methods **9**: 329–339. doi:10.4319/lom.2011.9.329

Clarke, K. R., P. J. Somerfield, and M. G. Chapman. 2006. On resemblance measures for ecological studies, including taxonomic dissimilarities and a zero-adjusted Bray–Curtis coefficient for denuded assemblages. J. Exp. Mar. Biol. Ecol. **330**: 55–80. doi:10.1016/j.jembe.2005.12.017

Collins, M., M. Sutherland, L. Bouwer, and others. 2019. Extremes, abrupt changes and managing risk. *In* H.-O. Pörtner and others [eds.], IPCC special report on the ocean and cryosphere in a changing climate. In press.

Dickman, E. M., J. M. Newell, M. J. González, and M. J. Vanni. 2008. Light, nutrients, and food-chain length constrain planktonic energy transfer efficiency across multiple trophic levels. Proc. Natl. Acad. Sci. U. S. A. **105**: 18408–18412. doi:10.1073/pnas.0805566105

D'Sa, E. J., I. Joshi, and B. Liu. 2018. Galveston Bay and coastal ocean optical-geochemical response to Hurricane Harvey from VIIRS ocean color. Geophys. Res. Lett. **45**: 10,579–10,589. doi:10.1029/2018GL079954

Du, J., K. Park, T. M. Dellapenna, and J. M. Clay. 2019*a*. Dramatic hydrodynamic and sedimentary responses in Galveston Bay and adjacent inner shelf to Hurricane Harvey. Sci. Total Environ. **653**: 554–564. doi:10.1016/j.scitotenv.2018.10.403

Du, J., K. Park, J. Shen, Y. J. Zhang, X. Yu, F. Ye, Z. Wang, and N. N. Rabalais. 2019*b*. A hydrodynamic model for Galveston Bay and the shelf in the northern Gulf of Mexico. Ocean Sci. **15**: 951–966. doi:10.5194/os-15-951-2019

Engels, B. 2015. XNomial: Exact goodness-of-fit test for multinomial data with fixed probabilities. https://CRAN.R-project.org/package=XNomial

Fiedler, P., J. Redfern, J. van Noord, C. Hall, R. Pitman, and L. Ballance. 2013. Effects of a tropical cyclone on a pelagic ecosystem from the physical environment to top predators. Mar. Ecol. Prog. Ser. **484**: 1–16. doi:10.3354/meps10378

Friedland, K. D., C. Stock, K. F. Drinkwater, and others. 2012. Pathways between primary production and fisheries yields of large marine ecosystems. PLoS One **7**: e28945. doi:10.1371/journal.pone.0028945

Gomez, F. A., S.-K. Lee, Y. Liu, F. J. Hernandez Jr., F. E. Muller-Karger, and J. T. Lamkin. 2018. Seasonal patterns in

phytoplankton biomass across the northern and deep Gulf of Mexico: A numerical model study. Biogeosciences **15**: 3561–3576. doi:10.5194/bg-15-3561-2018

Han, G., Z. Ma, and N. Chen. 2012. Hurricane Igor impacts on the stratification and phytoplankton bloom over the grand banks. J. Mar. Syst. **100–101**: 19–25. doi:10.1016/j.jmarsys.2012.03.012

Hogan, J. A., R. A. Feagin, G. Starr, and others. 2020. A research framework to integrate cross-ecosystem responses to tropical cyclones. Bioscience: **70**(6) 477–489. doi:10.1093/biosci/biaa034

Hu, C., and F. E. Muller-Karger. 2007. Response of sea surface properties to Hurricane dennis in the eastern Gulf of Mexico. Geophys. Res. Lett. **34**(7) L07606 https://doi.org/10.1029/2006GL028935

Hurlbert, S. H., and M. D. White. 1993. Experiments with freshwater invertebrate zooplanktivores: Quality of statistical analyses. Bull. Mar. Sci. **53**: 128–153.

IOC, SCOR, and IAPSO. 2010 The international thermodynamic equation of seawater: Calculation and use of thermodynamic properties.

Isles, P. D. F. 2020. The misuse of ratios in ecological stoichiometry. Ecology **101**: e03153. doi:10.1002/ecy.3153

Joint, I., P. Henriksen, G. Fonnes, D. Bourne, T. Thingstad, and B. Riemann. 2002. Competition for inorganic nutrients between phytoplankton and bacterioplankton in nutrient manipulated mesocosms. Aquat. Microb. Ecol. **29**: 145–159. doi:10.3354/ame029145

Jullien, S., C. E. Menkes, P. Marchesiello, and others. 2012. Impact of tropical cyclones on the heat budget of the South Pacific Ocean. J. Phys. Oceanogr. **42**: 1882–1906. doi:10.1175/JPO-D-11-0133.1

Kamykowski, D., and J. L. Bird. 1981. Phytoplankton associations with the variable nepheloid layer on the Texas continental shelf. Estuar. Coast. Shelf Sci **13**: 317–326.

Kelley, D., C. Richards. 2017. gsw: Gibbs Sea Water Functions Package. https://cran.r-project.org/web/packages/gsw/index.html

Lambert, C. D., T. S. Bianchi, and P. H. Santschi. 1999. Cross-shelf changes in phytoplankton community composition in the Gulf of Mexico (Texas shelf/slope): The use of plant pigments as biomarkers. Cont. Shelf Res. **19**: 1–21. doi:10.1016/S0278-4343(98)00075-2

Linacre, L., R. Lara-Lara, V. Camacho-Ibar, J. C. Herguera, C. Bazán-Guzmán, and V. Ferreira-Bartrina. 2015. Distribution pattern of picoplankton carbon biomass linked to mesoscale dynamics in the southern Gulf of Mexico during winter conditions. Deep Sea Res. Oceanogr. Res. Pap. **106**: 55–67. doi:10.1016/j.dsr.2015.09.009

Liu, H., M. Dagg, L. Campbell, and J. Urban-Rich. 2004. Picophytoplankton and bacterioplankton in the Mississippi River plume and its adjacent waters. Estuaries **27**: 147–156. doi:10.1007/BF02803568

Liu, B., D'Sa Eurico, J., and Joshi Ishan, D. 2019. Floodwater impact on Galveston Bay phytoplankton taxonomy, pigment composition and photo-physiological state following Hurricane Harvey from field and ocean color (Sentinel-3A OLCI) observations. Biogeosciences **16**: 1975–2001. http://dx.doi.org/10.5194/bg-16-1975-2019

López-Veneroni, D., L. A. Cifuentes, and D. Lopez-Veneroni. 1994. Transport of dissolved organic nitrogen in Mississippi River plume and Texas-Louisiana continental shelf near-surface waters. Estuaries **17**: 796. doi:10.2307/1352748

Lü, H., X. Zhao, J. Sun, G. Zha, J. Xi, and S. Cai. 2020. A case study of a phytoplankton bloom triggered by a tropical cyclone and cyclonic eddies. PLoS One **15**: e0230394. doi:10.1371/journal.pone.0230394

Marie, D., F. Partensky, S. Jacquet, and D. Vaulot. 1997. Enumeration and cell cycle analysis of natural populations of marine picoplankton by flow cytometry using the nucleic acid stain SYBR green I. Appl. Environ. Microbiol. **63**: 186–193.

Mcdonald, J. H. 2014. Handbook of biological statistics, 3rd ed. Sparky House Publishing.

McPherson, B. F., and R. L. Miller. 1987. The vertical attenuation of light in Charlotte Harbor, a shallow, subtropical estuary, South-Western Florida. Estuar. Coast. Shelf Sci **25**: 721–737. doi:10.1016/0272-7714(87)90018-7

Merritt-Takeuchi, A. M., and S. Chiao. 2013. Case studies of tropical cyclones and phytoplankton blooms over atlantic and pacific regions. Earth Interact. **17**: 1–19. doi:10.1175/2013EI000517.1

Morison, F., E. Harvey, G. Franzè, and S. Menden-Deuer. 2019. Storm-induced predator-prey decoupling promotes springtime accumulation of North Atlantic phytoplankton. Front. Mar. Sci. **6**:608. doi:10.3389/fmars.2019.00608

Ni, Z., X. Huang, and X. Zhang. 2015. Picoplankton and virioplankton abundance and community structure in Pearl River Estuary and Daya Bay, South China. J. Environ. Sci. **32**: 146–154. doi:10.1016/j.jes.2014.12.019

O'Dell, J. W. 1996. Determination of ammonia nitrogen by semi-automated colorimetry, p. 434–448.*In* Methods for the determination of metals in environmental samples. Elsevier.

Oksanen, J., F. G. Blanchet, M. Friendly and others. 2019. vegan: Community Ecology Package. https://CRAN.R-project.org/package=vegan

Owen, K. R. 2014. Flow cytometric investigation of the size spectrum of North Sea phytoplankton communities. Doctor of Philosophy. University of East Anglia.

Paerl, R. W., R. E. Venezia, J. J. Sanchez, and H. W. Paerl. 2020. Picophytoplankton dynamics in a large temperate estuary and impacts of extreme storm events. Sci. Rep. **10**: 22026. doi:10.1038/s41598-020-79157-6

Parsons, T., M. Yoshiaki, and C. Lalli. 1984. A manual of chemical & biological methods for seawater analysis. ScienceDirect, Elsevier.

Patrick, C. J., L. Yeager, A. R. Armitage, and others. 2020. A system level analysis of coastal ecosystem responses to hurricane impacts. Estuar. Coasts **43**: 943–959. doi:10.1007/s12237-019-00690-3

Peierls, B. L., R. R. Christian, and H. W. Paerl. 2003. Water quality and phytoplankton as indicators of hurricane impacts on a large estuarine ecosystem. Estuaries **26**: 1329–1343. doi:10.1007/BF02803635

R Core Team. 2016. R: A language and environment for statistical computing. R Foundation for Statistical Computing. Vienna, Austria. https://www.r-project.org/

Sanford, T. B., J. F. Price, J. B. Girton, and D. C. Webb. 2007. Highly resolved observations and simulations of the ocean response to a hurricane. Geophys. Res. Lett. **34**: L13604. doi:10.1029/2007GL029679

Steichen, J. L., J. M. Labonté, R. Windham, and others. 2020. Microbial, physical, and chemical changes in Galveston Bay following an extreme flooding event, Hurricane Harvey. Front. Mar. Sci. **7**:186. doi:10.3389/fmars.2020.00186

Strom, S. L. 2000. Bacterivory: Interactions between bacteria and their grazers. *In* D. L. Kirchman [ed.], Microbial ecology of the oceans. USA: Wiley-Liss.

ter Braak, C. J. F. 1986. Canonical correspondence analysis: A new eigenvector technique for multivariate direct gradient analysis. Ecology **67**: 1167–1179. doi:10.2307/1938672

Topor, Z., K. L. Robinson, and A. Turcu. 2020. Investigating seasonal succession patterns in mesozooplankton community structure following Hurricane Harvey. Front. Mar. Sci. **7**:462. doi:10.3389/fmars.2020.00462/full

Valiela, I., P. Peckol, C. D'Avanzo, and others. 1998. Ecological effects of major storms on coastal watersheds and coastal waters: Hurricane bob on Cape Cod. J. Coast. Res. **14**: 218–238.

Wachnicka, A., J. Browder, T. Jackson, W. Louda, C. Kelble, O. Abdelrahman, E. Stabenau, and C. Avila. 2020. Hurricane Irma's impact on water quality and phytoplankton communities in Biscayne Bay (Florida, USA). Estuar. Coasts **43**: 1217–1234. doi:10.1007/s12237-019-00592-4

Walker, N. D., R. R. Leben, and S. Balasubramanian. 2005. Hurricane-forced upwelling and chlorophyll *a* enhancement within cold-core cyclones in the Gulf of Mexico. Geophys. Res. Lett. **32**:L18610. doi:10.1029/2005GL023716

Wang, Y., F. Hammes, K. de Roy, W. Verstraete, and N. Boon. 2010. Past, present and future applications of flow cytometry in aquatic microbiology. Trends Biotechnol. **28**: 416–424. doi:10.1016/j.tibtech.2010.04.006

Welschmeyer, N. A. 1994. Fluorometric analysis of chlorophyll *a* in the presence of chlorophyll b and pheopigments. Limnol. Oceanogr. **39**: 1985–1992. doi:10.4319/lo.1994.39.8.1985

Wetz, M. S., and H. W. Paerl. 2008*a*. Estuarine phytoplankton responses to hurricanes and tropical storms with different characteristics (trajectory, rainfall, winds). Estuar. Coasts **31**: 419–429.

Wetz, M. S., and H. W. Paerl. 2008*b*. Impact of large storm events with different meteorological characteristics on estuarine ciliate biomass. J. Plankton Res. **30**: 551–557. doi:10.1093/plankt/fbn020

Williams, A. K., and A. Quigg. 2019. Spatiotemporal variability in autotrophic and heterotrophic microbial plankton abundances in a subtropical estuary (Galveston Bay, Texas). J. Coast. Res. **35**: 434–444. doi:10.2112/JCOASTRES-D-18-00004.1

Williams, A. K., A. S. McInnes, J. R. Rooker, and A. Quigg. 2015. Changes in microbial plankton assemblages induced by mesoscale oceanographic features in the northern Gulf of Mexico. PLoS One: **10**: e0138230. doi:10.1371/journal.pone.0138230

Xu, F., Y. Yao, L. Oey, and Y. Lin. 2017. Impacts of pre-existing ocean cyclonic circulation on sea surface chlorophyll-*a* concentrations off northeastern Taiwan following episodic typhoon passages: Cyclones impact on chl-*a* after typhoons. J. Geophys. Res. Oceans **122**: 6482–6497. doi:10.1002/2016JC012625

Yan, G., J. M. Labonté, A. Quigg, and K. Kaiser. 2020. Hurricanes accelerate dissolved organic carbon cycling in coastal ecosystems. Front. Mar. Sci. **7**:248. doi:10.3389/fmars.2020.00248

Zhang, J., and G. A. Berberian. 1997. Method 366.0 determination of dissolved silicate in estuarine and coastal watersby gas segmented continuous flow colorimetric analysis. EPA/600/R-15/010, EPA/600/R-15/010, U.S. Environmental Protection Agency.

Zhang, J., P. B. Ortner, and C. J. Fischer. 1997. Method 353.4 determination of nitrate and nitrite in estuarine and coastal waters by gas segmented continuous flow colorimetric analysis. EPA/600/R-15/012. EPA/600/R-15/012 U.S. Environmental Protection Agency.

Zhang, J.-Z., C. J. Fischer, and P. B. Ortner. 2000. Continuous flow analysis of phosphate in natural waters using hydrazine as a reductant. Int. J. Environ. Anal. Chem. **80**: 61–73. doi:10.1080/03067310108044386

Zheng, G. M., and D. Tang. 2007. Offshore and nearshore chlorophyll increases induced by typhoon winds and subsequent terrestrial rainwater runoff. Mar. Ecol. Prog. Ser. **333**: 61–74. doi:10.3354/meps333061

Zimmerman, C. F., and C. W. Keefe. 1997. Method 365.5 determination of orthophosphate in estuarine and coastal waters by automated colorimetric analysis. U.S. Environmental Protection Agency

Acknowledgments

This research was supported by the National Science Foundation (NSF Award #1760704), National Oceanic and Atmospheric Administration (NOAA Award #NA16NOS0120017), and National Academies of Sciences, Engineering, and Medicine Gulf Research Program (NASEM GRP Award #2000009659). The project was conducted as a part of larger collaborative group of institutions, and we acknowledge the work of our colleagues K. Robinson (University of Louisiana at Lafayette), and especially A. Schnetzer (North Carolina State University) and S. Geist (Texas A&M University-Corpus Christi) who provided valuable inputs to the

manuscript. We thank their lab members, and specifically S. McAskill, who collected samples on the September 2017 SEAMAP cruise. We also thank the crew of the NOAA Ship Ronald H. Brown, Point Sur, and Pelican and A. Jaegge, J. Babitch, M. Pathare, and G. Corradino for cruise-based sample collection. We thank L. Barbero (University of Miami, NOAA AOML) for physicochemical data from the July 2017 GOMECC-3 cruise and G. Zapfe (NOAA SEMFC) for data associated with the historical SEAMAP program dataset. Two anonymous reviewers substantially contributed to the improvement of the manuscript, and their insightful comments and recommendations were greatly appreciated.

Conflict of Interest

Coauthor Beth A. Stauffer is Member-at-Large of the ASLO Board of Directors.

Submitted 23 November 2020
Revised 05 April 2021
Accepted 12 April 2021

Associate editor: Susanne Menden-Deuer